Eur. Phys. J. B (2018) 91: 115
https://doi.org/10.1140/epjb/e2018-80673-0

THE EUROPEAN PHYSICAL JOURNAL B

Regular Article

Density correlations induced by temperature fluctuations in a photon gas

Roman Tomaschitz[a]

Sechsschimmelgasse 1/21-22, 1090 Vienna, Austria

Received 29 November 2017 / Received in final form 12 February 2018
Published online 13 June 2018

Abstract. The impact of angular temperature variations on the thermodynamic variables and real-space correlation functions of black-body radiation are analyzed. In particular, the effect of temperature fluctuations on the number density and energy density correlations of the cosmic microwave background (CMB) is studied. The angular temperature fluctuations are modeled by an isotropic and homogeneous Gaussian random field, whose autocorrelation function is defined on the unit sphere in momentum space. This temperature correlation function admits an angular Fourier transform which determines the density correlations in real space induced by temperature fluctuations. In the case of the CMB radiation, the multipole coefficients of the angular power spectrum defining the temperature correlation function have been measured by the Planck satellite. The fluctuation-induced perturbation of the equilibrium variables (internal energy, entropy, heat capacity and compressibility) can be quantified in terms of the measured multipole coefficients by expanding the partition function around the equilibrium state in powers of the temperature random field. The real-space density correlations can also be extracted from the measured temperature power spectrum. Both the number density and energy density correlations of the electromagnetic field are long-range, admitting power-law decay; in the case of the energy density correlation, the fluctuation-induced correlation overpowers the isotropic equilibrium correlation in the long-distance limit.

1 Introduction

We study angular-dependent temperature fluctuations in a photon gas, as occurring in the cosmic microwave background (CMB) radiation. The fluctuations distort the Planckian equilibrium density, resulting in a stationary non-equilibrium system. The aim is to quantify the impact of temperature fluctuations on the thermodynamic variables and real-space density correlation functions of the electromagnetic field. The angular temperature fluctuations are modeled by an isotropic Gaussian random field in momentum space. The pair correlation function of this random field admits a multipole expansion whose coefficients can be extracted from the temperature power spectrum, which has been measured with high accuracy in the case of the CMB radiation, up to multipoles of order $l \sim 2500$, cf. references [1–3].

As the photon gas is in stationary non-equilibrium due to the angular temperature variations, the thermodynamic variables such as internal energy and entropy are obtained as fluctuation averages and depend on the multipole coefficients of the temperature power spectrum. The effective temperature of the system, defined by the internal-energy derivative of entropy, deviates from the mean temperature; the difference, which is very small but still measurable in the case of the CMB radiation, can be expressed as a series of multipole coefficients and quantifies the deviation from the equilibrium state. The heat capacity and compressibility remain positive, as the equilibrium state is the leading order of the perturbative expansion in powers of the fluctuating temperature variable.

Angular temperature fluctuations in momentum space also affect the number density and energy density correlations in real space, especially the long-range asymptotics of the energy density correlation, which is dominated by temperature fluctuations. The real-space correlations of the CMB radiation are nearly constant at short distance and terminate in long-range power-law decay. There is an invertible one-to-one correspondence between the angular-dependent temperature correlation function on the unit sphere in momentum space and the frequency and distance dependent spectral kernels of the long-range density correlations.

Long-range correlations emerge in a variety of statistical systems and have been extensively studied, ranging from phase transitions in spin systems [4–7] and many-body problems [8,9] to interdisciplinary applications such

[a] e-mail: tom@geminga.org

as network theory [10], econophysics [11], linguistic text analysis [12], internet traffic flows [13] and earthquakes [14], to mention but a few.

In Section 2, we analyze the effect of angular temperature fluctuations on the thermodynamic variables by performing a perturbative expansion of the variables around the mean temperature in ascending powers of the temperature random field. We calculate the angular-averaged internal energy and entropy and then use the energy derivative of entropy to obtain the effective temperature $S_{,U} = 1/T_{\rm eff}$. The fluctuation corrections to the specific heat and compressibility of the photon gas are calculated from the entropy variable reparametrized with the effective temperature. The angular-averaged variances of the particle count and internal energy can be traced back to the spatially integrated correlation functions of the number and energy densities of the electromagnetic field discussed in Section 4.2.

In Section 3, we study the autocorrelation $\langle\delta T(\mathbf{k}_0)\delta T(\mathbf{k}_0')\rangle$ of the temperature random field on the unit sphere in momentum space. This Gaussian pair correlation is defined by an angular average over measured fluctuations $\delta T(\mathbf{k}_0)$, which renders $\langle\delta T(\mathbf{k}_0)\delta T(\mathbf{k}_0')\rangle$ isotropic, depending only on the polar angle $\mathbf{k}_0\mathbf{k}_0' = \cos\theta$. The temperature correlation function thus admits a multipole expansion on the unit sphere in terms of Legendre polynomials. In the case of the cosmic microwave background (CMB) radiation, the multipole coefficients C_l have been extracted from the measured angular fluctuations $\delta T(\mathbf{k}_0)$; in Section 3.1, we use a least-squares spectral fit to obtain an analytic representation of the multipole power spectrum C_l by a series of Gaussians, covering multipoles up to $l \sim 2500$ as measured by the Planck satellite [3]. In Section 3.2, we perform an angular Fourier transform of the pair correlation $\langle\delta T(\mathbf{k}_0)\delta T(\mathbf{k}_0')\rangle$, mapping the temperature correlation on the unit sphere $\mathbf{k}_0^2 = 1$ into an isotropic correlation function in real space. The latter is a frequency-dependent spectral kernel determining the impact of temperature fluctuations on spatial density correlations discussed in Sections 4–6. This transform of the temperature correlation $\langle\delta T(\mathbf{k}_0)\delta T(\mathbf{k}_0')\rangle$ into a real-space correlation function is invertible; the inversion is performed in Section 3.3.

In Sections 4–6, we study real-space density correlations of a photon gas, in particular the fluctuation-induced number and energy density correlations of the CMB radiation. In Section 4, we introduce the Fourier integrals and their fluctuation average defining the correlations. The latter can be decomposed into an isotropic component corresponding to an equilibrated photon gas and a fluctuation correction due to the angular temperature variation. We derive the spectral representation of the number and energy density correlations, whose spectral kernels are determined by the multipole coefficients of the temperature autocorrelation function, cf. Section 3. As a consistency check, we also show that the spatially integrated correlations reproduce the variances of number count and internal energy derived in Section 2.3.

In Section 5, we perform the frequency integration of the spectral kernels, obtaining explicit analytic expressions for the number density and energy density correlations in terms of Bessel series, and derive the short-distance limit of the correlations. The effect of temperature fluctuations on real-space correlation functions is illustrated by plots of the CMB number and energy density correlations, based on the temperature multipole spectrum discussed in Section 3.1. These plots depict the extended crossover from the short-distance limit to the asymptotic long-distance power-law correlations discussed in Section 6.

In Section 6, we study the large-distance asymptotics of the number density and energy density correlations, which exhibit power-law decay in this limit. The number density correlation generated by angular temperature fluctuations decays with the same power $1/r^4$ as the isotropic number density correlation of the equilibrium state. In contrast, the energy density correlation induced by angular fluctuations decays as $1/r^6$ and overpowers the isotropic energy density correlation of the equilibrated photon gas, which decays $\propto 1/r^8$ in the long-distance limit. In Section 7, we present our conclusions.

2 Angular temperature fluctuations in a photon gas

2.1 Fluctuation-averaged thermodynamic variables

Weakly anisotropic black-body radiation can be modeled by a Planck distribution with temperature variable $T + \delta T$, where T is the mean temperature and $\delta T(\mathbf{k}_0)$ a random field describing the angular temperature fluctuations. The anisotropic Planckian spectral number density reads

$$\mathrm{d}\rho(k,\mathbf{k}_0) = \frac{s}{(2\pi)^3}\frac{k^2\mathrm{d}k\mathrm{d}\Omega_{\mathbf{k}_0}}{\mathrm{e}^{H(k,\mathbf{k}_0,T)}-1},$$
$$H(k,\mathbf{k}_0,T) = \frac{k}{T+\delta T(\mathbf{k}_0)}, \qquad (1)$$

where $\mathrm{d}\Omega_{\mathbf{k}_0}$ is the surface element of the unit sphere $\mathbf{k}_0^2 = 1$ in momentum space. The two polarization degrees of the electromagnetic field are indicated by $s = 2$. ($\hbar = c = k_{\rm B} = 1$.) The temperature variable of an ideal photon gas is thus replaced by $T + \delta T(\mathbf{k}_0)$. As T is the mean temperature, the average of the temperature fluctuations over the unit sphere vanishes, $\int \delta T(\mathbf{k}_0)\mathrm{d}\Omega_{\mathbf{k}_0} = 0$. We treat $\delta T(\mathbf{k}_0)$ as an isotropic Gaussian random field with zero mean, $\langle\delta T(\mathbf{k}_0)\rangle = 0$, defined by a pair correlation function $\langle\delta T(\mathbf{k}_0)\delta T(\mathbf{k}_0')\rangle$ which only depends on the polar angle $\mathbf{k}_0\mathbf{k}_0' = \cos\theta$, cf. Section 3, so that $\delta_T^2 := \langle\delta T(\mathbf{k}_0)\delta T(\mathbf{k}_0)\rangle$ is constant.

The following derivations of the fluctuation-averaged thermodynamic variables based on spectral density (1) can easily be adapted to a Bose or Fermi gas of relativistic massive particles with angular-dependent temperature $T + \delta T(\mathbf{k}_0)$, defined by number density

$$\mathrm{d}\rho_{\rm B,F}(E,\mathbf{k}_0) = \frac{s}{(2\pi)^3}\frac{\sqrt{1-m^2/E^2}}{\mathrm{e}^{H(E,\mathbf{k}_0,T)+\alpha}\mp 1}E^2\mathrm{d}E\mathrm{d}\Omega_{\mathbf{k}_0}, \qquad (2)$$

with $H(E,\mathbf{k}_0,T)$ as in (1), dispersion relation $E = \sqrt{k^2+m^2}$, fugacity parameter $\alpha = -\log z$ and spin

multiplicity s. Here, we will focus on the spectral density (1) of a photon gas and use the microwave background radiation as example, since its Planckian shape and the angular temperature fluctuations have been measured with good precision over an extended frequency range. The relative fluctuations are of order $\delta T/T \sim 10^{-5}$ and thus allow a perturbative expansion of the thermodynamic variables around the mean temperature, so that a quantitative treatment of the density correlation functions studied in Sections 4 and 5 is possible.

By expanding the spectral density $\mathrm{d}\rho(k,\mathbf{k}_0)$ of blackbody radiation in $\delta T(\mathbf{k}_0)$, cf. (1), and performing the fluctuation average (indicated by angle brackets), we find

$$\langle \mathrm{d}\rho(k,\mathbf{k}_0)\rangle = \frac{s}{(2\pi)^3}\left[\frac{1}{\mathrm{e}^{k/T}-1}+\frac{1}{2}\left(\frac{1}{\mathrm{e}^{k/T}-1}\right)_{,T,T}\delta_T^2 + \mathrm{O}(\delta_T^4)\right]k^2\mathrm{d}k\mathrm{d}\Omega_{\mathbf{k}_0}. \tag{3}$$

The linear term in the expansion drops out due to homogeneity, $\langle \delta T(\mathbf{k}_0)\rangle = 0$. The specific number and energy densities and the pressure are obtained as

$$\begin{aligned}\frac{N}{V} &= n(T) = \int \langle \mathrm{d}\rho(k,\mathbf{k}_0)\rangle,\\ \frac{U}{V} &= u(T) = \int k\langle \mathrm{d}\rho(k,\mathbf{k}_0)\rangle,\end{aligned} \tag{4}$$

and $P = u/3$. The temperature derivatives in (3) (and in the subsequent averages) are performed after the elementary integrations,

$$\begin{aligned}u(T) &= \hat{\sigma}T^4\left(1+6\frac{\delta_T^2}{T^2}\right), \quad \hat{\sigma} := \frac{4\pi s}{(2\pi)^3}\frac{\pi^4}{15},\\ n(T) &= \frac{4\pi s}{(2\pi)^3}2\zeta(3)T^3\left(1+3\frac{\delta_T^2}{T^2}\right).\end{aligned} \tag{5}$$

As for the CMB radiation, $\delta_T^2/T^2 = 1.770\times 10^{-9}$, with a mean temperature of $T = 2.725$ K, see Section 3.1.

The partition function corresponding to spectral density (1) is

$$\begin{aligned}\log Z &= -\frac{sV}{(2\pi)^3}\int \log(1-\mathrm{e}^{-H(k,\mathbf{k}_0,T)})k^2\mathrm{d}k\mathrm{d}\Omega_{\mathbf{k}_0}\\ &= \frac{V}{3}\int H_{,k}(k,\mathbf{k}_0,T)k\mathrm{d}\rho(k,\mathbf{k}_0),\end{aligned} \tag{6}$$

where we have used integration by parts. The fluctuation average of $\log Z$ is performed by expanding the integrand $H_{,k}k\mathrm{d}\rho = H\mathrm{d}\rho$ to second order in the random field $\delta T(\mathbf{k}_0)$ and by averaging using $\langle \delta T(\mathbf{k}_0)\rangle = 0$ and the shortcut $\langle \delta T(\mathbf{k}_0)\delta T(\mathbf{k}_0)\rangle = \delta_T^2$,

$$\langle H\mathrm{d}\rho\rangle = \frac{s}{(2\pi)^3}k^3\mathrm{d}k\mathrm{d}\Omega_{\mathbf{k}_0}\frac{1}{T}\left\{\frac{1}{\mathrm{e}^{k/T}-1}+\left[\frac{1}{2}\left(\frac{1}{\mathrm{e}^{k/T}-1}\right)_{,T,T} - \frac{1}{T}\left(\frac{1}{\mathrm{e}^{k/T}-1}\right)_{,T}+\frac{1}{T^2}\frac{1}{\mathrm{e}^{k/T}-1}\right]\delta_T^2\right\}. \tag{7}$$

In this way, we arrive at

$$\begin{aligned}\langle \log Z\rangle &= \frac{V}{3}\int\langle H\mathrm{d}\rho\rangle,\\ \int\langle H\mathrm{d}\rho\rangle &= \frac{4\pi s}{(2\pi)^3}\frac{\pi^4}{15}T^3\left(1+3\frac{\delta_T^2}{T^2}\right).\end{aligned} \tag{8}$$

The entropy can be averaged in like manner,

$$\frac{S}{V} = s(T) = \frac{1}{V}\langle \log Z\rangle + \int\langle H(k,\mathbf{k}_0,T)\mathrm{d}\rho(k,\mathbf{k}_0)\rangle, \tag{9}$$

and we use (8) to find $s(T) = 4\langle \log Z\rangle/V$ or

$$s(T) = \frac{4}{3}\hat{\sigma}T^3\left(1+3\frac{\delta_T^2}{T^2}\right), \quad \hat{\sigma} := \frac{4\pi s}{(2\pi)^3}\frac{\pi^4}{15}. \tag{10}$$

The above expansions (and the subsequent ones) are up to terms of $\mathrm{O}(\delta_T^4/T^4)$. The systematic expansion in powers of the random field $\delta T(\mathbf{k}_0)$ (performed in (3) and (7) up to second order) is not to be considered as an approximation, but rather as the proper definition of the integrands, since $\delta T(\mathbf{k}_0)$ is only defined by its correlation functions; higher-order correlations are linear combinations of products of $\langle \delta T(\mathbf{k}_0)\delta T(\mathbf{k}_0')\rangle$.

2.2 Effective temperature, heat capacity and compressibility

The (U,V,N) parametrization of entropy $S/V = s(T)$ is $S = Vs(u^{-1}(U/V))$. The U derivative thereof defines the effective temperature of a photon gas in stationary non-equilibrium [15],

$$S_{,U}(U,V) = \frac{s'(T)}{u'(T)} = \frac{1}{T_{\mathrm{eff}}}, \tag{11}$$

so that

$$\begin{aligned}T_{\mathrm{eff}} &:= d(T) = T\left(1+2\frac{\delta_T^2}{T^2}\right),\\ T &= T_{\mathrm{eff}}\left(1-2\frac{\delta_T^2}{T_{\mathrm{eff}}^2}\right).\end{aligned} \tag{12}$$

The entropy in (T_{eff},V) representation reads $S(T_{\mathrm{eff}},V) = Vs(d^{-1}(T_{\mathrm{eff}}))$, with the shortcut $d(T)$ in (12), and the effective temperature derivative is $S_{,T_{\mathrm{eff}}}(T_{\mathrm{eff}},V) = Vs'(T)/d'(T)$. At constant volume, the heat differential $\mathrm{d}Q$ coincides with the internal energy differential $\mathrm{d}U = T_{\mathrm{eff}}\mathrm{d}S$, cf. (11), so that $\mathrm{d}Q = T_{\mathrm{eff}}S_{,T_{\mathrm{eff}}}\mathrm{d}T_{\mathrm{eff}}$. Accordingly, the isochoric heat capacity reads, cf. (10) and (12),

$$\begin{aligned}C_V &= T_{\mathrm{eff}}S_{,T_{\mathrm{eff}}} = Vd\frac{s'}{d'} = 4\hat{\sigma}VT^3(1+5\frac{\delta_T^2}{T^2}),\\ \hat{\sigma} &:= \frac{4\pi s}{(2\pi)^3}\frac{\pi^4}{15}.\end{aligned} \tag{13}$$

By inverting the pressure, $P = p(T) = u/3$, cf. (5), and substituting into $S/V = s(T)$, we find the (P,V)

representation of entropy, $S(P,V) = Vs(p^{-1}(P))$. Thus, $V(P,S) = S/s(p^{-1}(P))$, which defines the adiabatic compressibility $\kappa_S = -V_{,P}/V$ or

$$\kappa_S = \frac{1}{s}\frac{s'}{p'} = \frac{9}{4}\frac{1}{\hat{\sigma}T^4}\left(1 - 5\frac{\delta_T^2}{T^2}\right), \tag{14}$$

where we used (5) and (10). Since the thermal equation $P = u/3$ is independent of volume (see (5)), due to the absence of a chemical potential in the Planck distribution (1), the isobaric specific heat, the isobaric expansion coefficient and the isothermal compressibility are not defined for a photon gas. The δ_T^2/T^2 corrections in the above equations indicate the deviation from equilibrium due to temperature fluctuations; δ_T^2 is a shortcut for the angular average $\langle \delta T(\mathbf{k}_0)\delta T(\mathbf{k}_0)\rangle$, which is a constant independent of the unit wave vector $\mathbf{k}_0$. A specific example, the CMB radiation, will be discussed in the subsequent sections, where we estimate δ_T^2/T^2 from measured temperature fluctuations.

2.3 Variances of particle count and internal energy

The variances of the particle number and internal energy are $\langle \Delta N^2\rangle_{\mathrm{q}} = \langle N^2\rangle_{\mathrm{q}} - \langle N\rangle_q^2$, where $\Delta N = N - \langle N\rangle_q$, and analogously for $\langle \Delta U^2\rangle_{\mathrm{q}}$; the quantum statistical average is denoted by an angle bracket with a subscript q to distinguish it from the subsequent fluctuation average, also indicated by angle brackets. We find

$$\langle \Delta N^2\rangle_{\mathrm{q}} = \frac{sV}{(2\pi)^3}\int \frac{\mathrm{e}^{H(k,\mathbf{k}_0,T)}}{(\mathrm{e}^{H(k,\mathbf{k}_0,T)}-1)^2}k^2\mathrm{d}k\mathrm{d}\Omega_{\mathbf{k}_0}, \tag{15}$$

and analogously $\langle \Delta U^2\rangle_{\mathrm{q}}$ with k^2 replaced by k^4. To derive this, we replace $\log(1-\mathrm{e}^{-H})$ in the integrand of partition function (6) by $\log(1-\mathrm{e}^{-H-\alpha-\varepsilon k})$ and calculate $\langle \Delta N^2\rangle_{\mathrm{q}} = (\log Z)_{,\alpha,\alpha}$ and $\langle \Delta U^2\rangle_{\mathrm{q}} = (\log Z)_{,\varepsilon,\varepsilon}$ at $\alpha = \varepsilon = 0$, cf. reference [16].

To average the variance $\langle \Delta N^2\rangle_{\mathrm{q}}$ in (15) over the temperature fluctuations, we expand the integrand in $\delta T(\mathbf{k}_0)$ and average the $\delta T(\mathbf{k}_0)$ products as done in (3) and (7),

$$\left\langle \frac{\mathrm{e}^{H(k,\mathbf{k}_0,T)}}{(\mathrm{e}^{H(k,\mathbf{k}_0,T)}-1)^2}\right\rangle = \frac{\mathrm{e}^{k/T}}{(\mathrm{e}^{k/T}-1)^2} + \frac{1}{2}\left(\frac{\mathrm{e}^{k/T}}{(\mathrm{e}^{k/T}-1)^2}\right)_{,T,T}\delta_T^2 + \mathrm{O}(\delta_T^4). \tag{16}$$

Replacing the ratio in (15) by this average, we find the angular-averaged variances $\langle\langle \Delta N^2\rangle_{\mathrm{q}}\rangle = \langle\langle N^2\rangle_{\mathrm{q}}\rangle - \langle\langle N\rangle_q^2\rangle$ and $\langle\langle \Delta U^2\rangle_{\mathrm{q}}\rangle$ as

$$\langle\langle \Delta N^2\rangle_{\mathrm{q}}\rangle = \frac{4\pi sV}{(2\pi)^3}\frac{\pi^2}{3}T^3\left(1+3\frac{\delta_T^2}{T^2}\right),$$
$$\langle\langle \Delta U^2\rangle_{\mathrm{q}}\rangle = \frac{4\pi sV}{(2\pi)^3}\frac{4\pi^4}{15}T^5\left(1+10\frac{\delta_T^2}{T^2}\right). \tag{17}$$

The fluctuation averages $\langle\langle N\rangle_q^2\rangle$ and $\langle\langle U\rangle_q^2\rangle$ read

$$\langle\langle N\rangle_q^2\rangle = V^2\int\langle \mathrm{d}\rho(k,\mathbf{k}_0)\mathrm{d}\rho(k',\mathbf{k}_0')\rangle,$$
$$\langle\langle U\rangle_q^2\rangle = V^2\int kk'\langle \mathrm{d}\rho(k,\mathbf{k}_0)\mathrm{d}\rho(k',\mathbf{k}_0')\rangle. \tag{18}$$

In Section 5, we will obtain these averages as the $r = 0$ limit of the correlation functions $\langle G_n(r)\rangle$ of the number and energy densities, $\langle\langle N\rangle_q^2\rangle = sV^2\langle G_{n=0}(r=0)\rangle$ and $\langle\langle U\rangle_q^2\rangle = sV^2\langle G_{n=1}(r=0)\rangle$, see (40) and (64). In (4) and (5), we calculated $\langle\langle N\rangle_q\rangle = Vn(T)$ and $\langle\langle U\rangle_q\rangle = Vu(T)$. The average $\langle\langle N\rangle_q^2\rangle$ factorizes into $\langle\langle N\rangle_q\rangle^2$ and analogously $\langle\langle U\rangle_q^2\rangle$.

3 Temperature autocorrelation

3.1 Multipole coefficients

We consider the isotropic average of a fluctuating temperature field $\delta T(\mathbf{k}_0)$ on the unit sphere in momentum space [17],

$$\langle \delta T(\mathbf{k}_0)\delta T(\mathbf{k}_0')\rangle = \frac{1}{8\pi^2}\iint \delta T(\mathbf{q}_0)\delta T(\mathbf{q}_0') \times\delta(\mathbf{q}_0\mathbf{q}_0' - \mathbf{k}_0\mathbf{k}_0')\mathrm{d}\Omega_{\mathbf{q}_0}\mathrm{d}\Omega_{\mathbf{q}_0'}, \tag{19}$$

which only depends on the polar angle $\mathbf{k}_0\mathbf{k}_0' = \cos\theta$. $\mathrm{d}\Omega_{\mathbf{q}_0}$ and $\mathrm{d}\Omega_{\mathbf{q}_0'}$ are the solid angle elements of $\mathbf{q}_0$ and $\mathbf{q}_0'$; the subscript zero denotes unit vectors. The average (19) is performed with the normalized density $\delta(\mathbf{q}_0\mathbf{q}_0' - \cos\theta)\mathrm{d}\Omega_{\mathbf{q}_0}\mathrm{d}\Omega_{\mathbf{q}_0'}/(8\pi^2)$. The field $\delta T(\mathbf{k}_0)$ is a measured field configuration on the unit sphere.

The random field $\delta T(\mathbf{k}_0)$ is assumed to be homogeneous, $\langle \delta T(\mathbf{k}_0)\rangle = 0$, and Gaussian, defined by the isotropic pair correlation function (19), which can be expanded in Legendre polynomials,

$$\langle \delta T(\mathbf{k}_0)\delta T(\mathbf{k}_0')\rangle = \frac{1}{2\pi}\sum_{l=0}^{\infty}(l+1/2)C_lP_l(\mathbf{k}_0\mathbf{k}_0'), \tag{20}$$

where the multipole coefficients are defined by

$$C_l = \int\langle \delta T(\mathbf{k}_0)\delta T(\mathbf{k}_0')\rangle P_l(\mathbf{k}_0\mathbf{k}_0')\mathrm{d}\Omega_{\mathbf{k}_0'}, \tag{21}$$

and $\mathrm{d}\Omega_{\mathbf{k}_0'} = \sin\theta\mathrm{d}\theta\mathrm{d}\varphi$ is the surface element on the unit sphere. Since $P_0(\cos\theta) = 1$, $P_n(1) = 1$, with $\mathbf{k}_0\mathbf{k}_0' = \cos\theta$, we find

$$\delta_T^2 := \langle \delta T^2(\mathbf{k}_0)\rangle = \frac{1}{2\pi}\sum_{l=0}^{\infty}(l+1/2)C_l, \tag{22}$$

which determines the effective temperature, cf. (12), and the fluctuation corrections δ_T^2/T^2 of the thermodynamic variables in Section 2. Since $\langle \delta T(\mathbf{k}_0)\delta T(\mathbf{k}_0')\rangle$ only depends

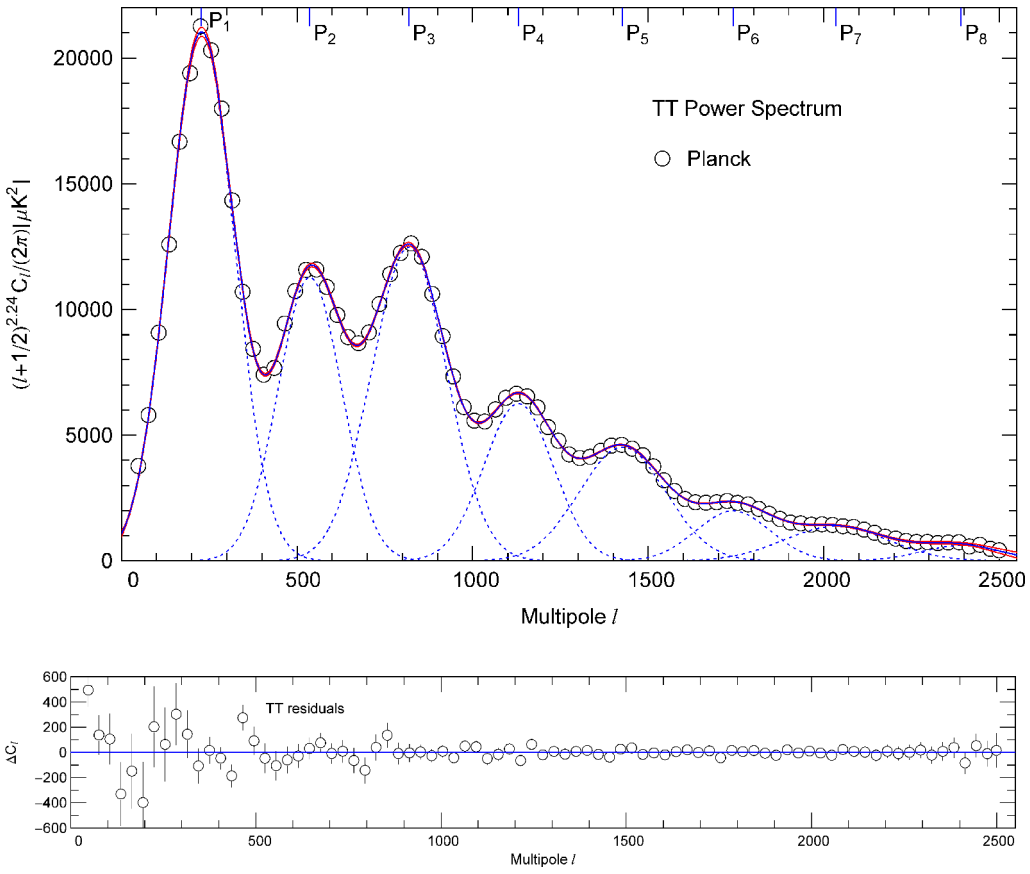

Fig. 1. Temperature power spectrum $\langle TT\rangle$ of the CMB radiation. Data points (binned) from reference [3]. The least-squares fit of the multipole coefficients C_l is depicted as solid blue curve, which is almost coincident with the 1σ error band (red solid curves), also see the close-up of the low-l spectrum in Figure 2, where the fit is better distinguishable from the error band. The fit of the C_l is performed with a series of eight Gaussians (blue dotted curves), rescaled with a power law, $(l+1/2)^{2+\mu}C_l/(2\pi) = \sum_{n=1}^{8} a_n \exp[-(l-b_n)^2/(2\sigma_n^2)]$. The fit parameters are the power-law exponent $\mu = 0.24009$ and the parameters a_n, b_n and σ_n of the Gaussians, cf. Table 1. The location b_n of the peaks is indicated on the upper abscissa by the approximately equidistant P_n. Structurally similar power spectra have been obtained for angular intensity fluctuations of cosmic rays [18,19], consisting of a main peak followed by a decaying oscillatory tail with nearly equidistant maxima. The residuals of the χ^2 fit are depicted in the lower panel. $\chi^2/\mathrm{dof} = 1.03$.

on the product $\mathbf{k}_0\mathbf{k}_0' = \cos\theta$, the multipole coefficients (21) are independent of $\mathbf{k}_0$. Moreover,

$$C_l = \frac{1}{4\pi}\iint \delta T(\mathbf{k}_0)\delta T(\mathbf{k}_0')P_l(\mathbf{k}_0\mathbf{k}_0')\mathrm{d}\Omega_{\mathbf{k}_0'}\mathrm{d}\Omega_{\mathbf{k}_0}. \quad (23)$$

That is, instead of the average (20), we can directly use the measured fluctuation field to obtain the multipole moments [2,3]. In fact, by inserting (23) into (20) and applying the completeness relation for Legendre polynomials,

$$\sum_{l=0}^{\infty}(l+1/2)P_l(\mathbf{q}_0\mathbf{q}_0')P_l(\mathbf{p}_0\mathbf{p}_0') = \delta(\mathbf{q}_0\mathbf{q}_0' - \mathbf{p}_0\mathbf{p}_0'), \quad (24)$$

we recover $\langle\delta T(\mathbf{k}_0)\delta T(\mathbf{k}_0')\rangle$ as defined in (19). Alternatively, we can substitute (19) into (21) and interchange integrations to arrive at representation (23) of the C_l. Also, we may just insert the completeness relation (24) into (19) and compare with (20) to obtain (23). Since the mean temperature T is defined by $\int \delta T(\mathbf{k}_0)\mathrm{d}\Omega_{\mathbf{k}_0} = 0$, see Section 2.1, we have $C_0 = 0$, cf. (23).

In the case of the CMB radiation, an analytic representation of the multipole coefficients C_l, $l \geq 1$, can be obtained from a least-squares fit of the measured multipole spectrum, see Figures 1 and 2. The fit consists of a series of eight Gaussians and an overall power-law scale factor,

$$(l+1/2)^{2+\mu}\frac{C_l}{2\pi} = \sum_{n=1}^{8} a_n \exp\left(-\frac{(l-b_n)^2}{2\sigma_n^2}\right). \quad (25)$$

The power-law exponent μ and the parameters a_n, b_n, σ_n defining the Gaussians are extracted from the spectral fit, which is based on $l \sim 2500$ measured multipole coefficients, cf. the caption of Table 1. In the numerical evaluation of the number and energy density correlations

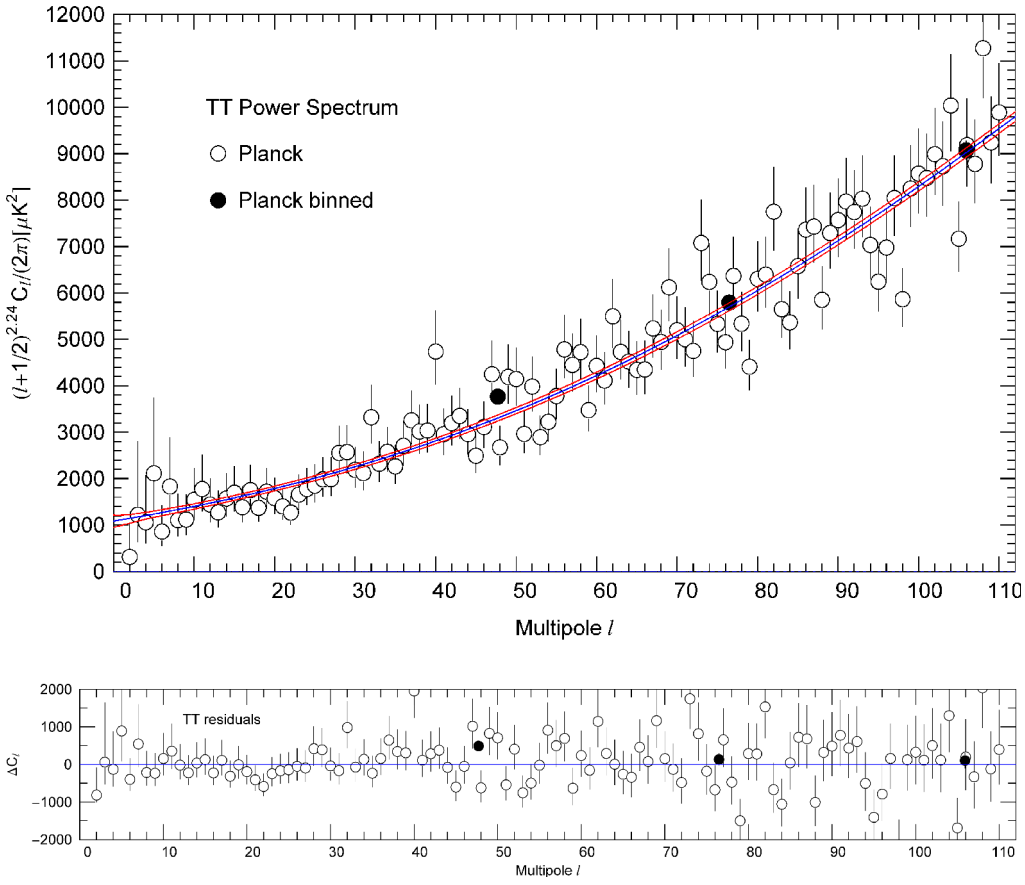

Fig. 2. Close-up of the low-l temperature power spectrum ($2 \leq l \leq 110$) in Figure 1. Data points and notation as in Figure 1. (The filled black circles are the first three binned data points in Fig. 1.) The solid blue curve is the χ^2 fit of the multipole coefficients C_l, the 1σ error band is depicted in red. Despite the large error bars of the data points at low l due to cosmic variance, the error band defined by the least-squares fit is quite narrow. The fit depicted here coincides with the ascending slope of the first peak P_1 in Figure 1; the subsequent peaks do not contribute in this l range. The power-law rescaling of the C_l is indicated in the caption of Figure 1; the power-law exponent $\mu = 0.24009$ is mainly determined by the low-l data points depicted here. When calculating spatial correlation functions, we use the analytic representation of the C_l defined by the rescaled series of eight Gaussians in (25) and Figure 1. The residuals are depicted in the lower panel.

studied in Sections 4–6, we will use this analytic representation of the multipole coefficients, with parameters listed in Table 1. We can sum the series δ_T^2 in (22), with $C_0 = 0$ and the $C_{l\geq 1}$, in (25) substituted, to find $\delta_T^2/T^2 = 1.770 \times 10^{-9}$, where $T = (2.7255 \pm 0.0006)$ K is the CMB mean temperature. The pair correlation function $\langle \delta T(\mathbf{k}_0)\delta T(\mathbf{k}_0')\rangle$ defining the random field is obtained in like manner, by substituting the $C_{l\geq 1}$ in (25) into the Legendre series (20).

Based on the analytic fit (25), we find the intrinsic dipole $C_1/T^2 = 3.806 \times 10^{-10}$ (after subtraction of the dipole generated by the motion of the Earth in the CMB rest frame) and the quadrupole coefficient $C_2/T^2 = 1.244 \times 10^{-10}$. δ_T^2 is the cosmic variance of the mean temperature T, so that the standard deviation $\delta_T = 1.15 \times 10^{-4}$ K has to be added in square to the above indicated measurement error of 6×10^{-4} K. That is, the CMB mean temperature at different locations in the universe varies within δ_T.

3.2 Angular Fourier transform of temperature correlations

First, we note the orthogonality relation for Legendre polynomials on the unit sphere [20],

$$\int P_n(\mathbf{k}_0\mathbf{q}_0)P_l(\mathbf{k}_0\mathbf{p}_0)\mathrm{d}\Omega_{\mathbf{k}_0} = \delta_{nl}\frac{2\pi}{l+1/2}P_l(\mathbf{p}_0\mathbf{q}_0), \quad (26)$$

and the expansion of an exponential into Legendre polynomials [21],

$$\mathrm{e}^{\mathrm{i}\mathbf{k}\mathbf{p}} = \sum_{l=0}^{\infty}\mathrm{i}^l(2l+1)j_l(kp)P_l(\mathbf{k}_0\mathbf{p}_0). \quad (27)$$

The $j_n(x) = \sqrt{\pi/(2x)}J_{n+1/2}(x)$ are spherical Bessel functions, in particular $j_0(x) = \sin x/x$. Using (26) and (27),

Table 1. Fit parameters of the multipole coefficients C_l of the CMB temperature autocorrelation $\langle TT\rangle$, cf. (20). The χ^2 fit depicted in Figures 1 and 2 is performed with a series of eight Gaussians rescaled with a power law, $(l+1/2)^{2+\mu}C_l/(2\pi) = \sum_{n=1}^{8} a_n \exp[-(l-b_n)^2/(2\sigma_n^2)]$. The power-law exponent $\mu = 0.24009$ and the listed amplitudes a_n, peaks b_n (labeled P_n in Fig. 1) and RMS widths σ_n of the Gaussians are fitting parameters. The peaks b_n are approximately equidistant. The least-squares fit is based on 2507 data points C_l, $2 \leq l \leq 2508$, cf. reference [3]; the low-l multipole coefficients up to $l = 110$ are depicted in Figure 2, the binned high-l spectrum above $l = 30$ is shown in Figure 1. $\chi^2/\mathrm{dof} = 2555.4/2482$.

n	$a_n[\mu\mathrm{K}^2]$	b_n	σ_n
1	21 015	227.38	93.426
2	11 276	536.28	90.761
3	12 474	818.60	107.11
4	6258.0	1130.1	98.473
5	4530.1	1426.7	123.24
6	1993.0	1741.6	105.28
7	1378.0	2034.3	148.28
8	615.01	2390.9	113.98

we find

$$\int P_n(\mathbf{k}_0\mathbf{q}_0)\mathrm{e}^{\mathrm{i}\mathbf{k}\mathbf{x}}\mathrm{d}\Omega_{\mathbf{k}_0}\mathrm{e}^{-\mathrm{i}\mathbf{q}\mathbf{x}'}\mathrm{d}\Omega_{\mathbf{q}_0} = (4\pi)^2 j_n(kr)j_n(qr') \times P_n(\mathbf{x}_0\mathbf{x}_0'), \quad (28)$$

If $\mathbf{x}_0' = \mathbf{x}_0$, we can drop $P_n(\mathbf{x}_0\mathbf{x}_0')$, since $P_n(1) = 1$.

The angular Fourier transform of the correlation function $\langle\delta T(\mathbf{k}_0)\delta T(\mathbf{k}_0')\rangle$ in (20) is

$$\delta G(r;k,k') = \frac{1}{(4\pi)^2}\int \langle\delta T(\mathbf{k}_0)\delta T(\mathbf{k}_0')\rangle \times \mathrm{e}^{\mathrm{i}\mathbf{k}\mathbf{x}}\mathrm{d}\Omega_{\mathbf{k}_0}\mathrm{e}^{-\mathrm{i}\mathbf{k}'\mathbf{x}}\mathrm{d}\Omega_{\mathbf{k}_0'}. \quad (29)$$

By applying (28), we obtain

$$\delta G(r;k,k') = \frac{1}{2\pi}\sum_{l=0}^{\infty}(l+1/2)C_l j_l(kr)j_l(k'r), \quad (30)$$

which is the real-space counterpart to the temperature correlation (20) on the unit sphere in momentum space.

3.3 Inversion of the angular Fourier transform

We show that the angular Fourier transform (29) is invertible, so that there is an unambiguous one-to-one correspondence between the temperature correlations $\langle\delta T(\mathbf{k}_0)\delta T(\mathbf{k}_0')\rangle$ on the unit sphere in momentum space and the correlation function $\delta G(r;k,k')$ in real space, cf. (20) and (30). (In Sect. 4, we will relate the number and energy density correlations of a photon gas to $\delta G(r;k,k')$.)

The inversion of transform (29) is

$$\langle\delta T(\mathbf{k}_0)\delta T(\mathbf{k}_0')\rangle = \frac{pkk'}{\pi^2}\int \delta G(r;k,k')\mathrm{e}^{\mathrm{i}\mathbf{p}\mathbf{x}}\mathrm{d}\mathbf{x} = \frac{4kk'}{\pi}\int_0^{\infty}\delta G(r;k,k')\sin(pr)r\mathrm{d}r, \quad (31)$$

where

$$p = |\mathbf{k}-\mathbf{k}'| = \sqrt{k^2+k'^2-2kk'\cos\theta}, \quad (32)$$

with $\mathbf{k}_0\mathbf{k}_0' = \cos\theta$ and $|\cos\theta| < 1$. If $\cos\theta = \pm 1$, a factor of 2 has to be added on the right-hand side of (31). $\langle\delta T(\mathbf{k}_0)\delta T(\mathbf{k}_0')\rangle$ is independent of k, k'. This inversion follows from the discontinuous Bessel integral

$$\int_0^{\infty} j_l(kr)j_l(k'r)\sin(pr)r\mathrm{d}r = \frac{\pi}{4kk'}P_l(\cos\theta), \quad (33)$$

with $p(\cos\theta)$ as in (32) and $|\cos\theta| < 1$. At the boundaries $\cos\theta = \pm 1$, the factor of 4 is replaced by 8. Outside the p range parametrized by $\cos\theta$, integral (33) vanishes identically. Derivations of the Bessel integrals employed in this section can be found in reference [22]; also see references [23–25] for alternative derivations. The inversion of (33) is

$$j_l(kr)j_l(k'r) = \frac{1}{2}\int_0^{\pi} P_l(\cos\theta)\frac{\sin(pr)}{pr}\sin\theta\mathrm{d}\theta, \quad (34)$$

since, by way of (26) and (27),

$$\frac{\sin(pr)}{pr} = \frac{1}{4\pi}\int \mathrm{e}^{\mathrm{i}(k\mathbf{k}_0-k'\mathbf{k}_0')r\mathbf{x}_0}\mathrm{d}\Omega_{\mathbf{x}_0} = \sum_{l=0}^{\infty}(2l+1)j_l(kr)j_l(k'r)P_l(\mathbf{k}_0\mathbf{k}_0'), \quad (35)$$

so that we may write, instead of (29),

$$\delta G(r;k,k') = \frac{1}{2}\int_0^{\pi}\langle\delta T(\mathbf{k}_0)\delta T(\mathbf{k}_0')\rangle\frac{\sin(pr)}{pr}\sin\theta\mathrm{d}\theta, \quad (36)$$

which is the inversion of the transform (31). The average $\langle\delta T(\mathbf{k}_0)\delta T(\mathbf{k}_0')\rangle$ only depends on $\mathbf{k}_0\mathbf{k}_0' = \cos\theta$, see (20), and $p(\cos\theta)$ as in (32).

4 Real-space correlations: number density and energy density correlations

4.1 Effect of temperature fluctuations on correlation functions

Spatial correlations of number and energy density fluctuations of the electromagnetic field are defined by the

quantum statistical average, cf. reference [26],

$$\rho_n(\mathbf{r}) := \langle(\hat\rho_n(\mathbf{x}) - \langle\hat\rho_n(\mathbf{x})\rangle_q)(\hat\rho_n(\mathbf{y}) - \langle\hat\rho_n(\mathbf{y})\rangle_q)\rangle_q = \frac{1}{(2\pi)^3}\int k'^n \mathrm{e}^{-\mathrm{i}\mathbf{k}'(\mathbf{x}-\mathbf{y})}\mathrm{d}\mathbf{k}' \times \int k^n \mathrm{e}^{\mathrm{i}\mathbf{k}(\mathbf{x}-\mathbf{y})}\mathrm{d}\rho(k,\mathbf{k}_0) + G_n(r), \quad (37)$$

where $\mathbf{r} = \mathbf{x} - \mathbf{y}$, and $\mathrm{d}\rho(k,\mathbf{k}_0)$ is the spectral density (1). The number density and energy density operators are denoted by $\hat\rho_{n=0}(\mathbf{x})$ and $\hat\rho_{n=1}(\mathbf{x})$, respectively. The pair correlation function $G_n(r)$ is a squared Fourier transform,

$$G_n(r) = \frac{s}{(2\pi)^6}\int \frac{k^n \mathrm{e}^{\mathrm{i}\mathbf{k}\mathbf{r}}\mathrm{d}\mathbf{k}}{\mathrm{e}^{H(k,\mathbf{k}_0,T)}-1}\int \frac{k'^n \mathrm{e}^{-\mathrm{i}\mathbf{k}'\mathbf{r}}\mathrm{d}\mathbf{k}'}{\mathrm{e}^{H(k',\mathbf{k}'_0,T)}-1}, \quad (38)$$

with $H(k,\mathbf{k}_0,T)$ as in (1). $s = 2$ accounts for the polarization degrees. The first integral in (37) is divergent; in the case of number density correlations ($n = 0$), equation (37) can be written as $\langle\rho_{n=0}(\mathbf{r})\rangle = \delta(\mathbf{r})\int \mathrm{d}\rho(k,\mathbf{k}_0) + G_{n=0}(r)$. The proper correlation function is $G_n(r)$, which is finite at $r = 0$. The meaning of the zero-point divergence in (37) is discussed in Section 4.2. A derivation of (38) in terms of creation and annihilation operators can be found in reference [26], for free Bose ensembles.

The fluctuation average $\langle\rho_n(\mathbf{r})\rangle$ of the correlation (37) reads

$$\langle\rho_n(\mathbf{x})\rangle = \frac{1}{(2\pi)^3}\int k'^n \mathrm{e}^{-\mathrm{i}\mathbf{k}'\mathbf{x}}\mathbf{d}\mathbf{k}' \times \int k^n \mathrm{e}^{\mathrm{i}\mathbf{k}\mathbf{x}}\langle\mathrm{d}\rho(k,\mathbf{k}_0)\rangle + \langle G_n(r)\rangle, \quad (39)$$

where we have put $\mathbf{y} = 0$, $\mathbf{r} = \mathbf{x}$, using homogeneity. $\langle\mathrm{d}\rho(k,\mathbf{k}_0)\rangle$ is the averaged spectral density (3) and $\langle G_n(r)\rangle$ denotes the averaged pair correlation function

$$\langle G_n(r)\rangle = \frac{s}{(2\pi)^6}\int\left\langle \frac{1}{\mathrm{e}^{H(k,\mathbf{k}_0,T)}-1}\frac{1}{\mathrm{e}^{H(k',\mathbf{k}'_0,T)}-1}\right\rangle \times \mathrm{e}^{\mathrm{i}\mathbf{k}\mathbf{x}}k^n\mathrm{d}\mathbf{k}\mathrm{e}^{-\mathrm{i}\mathbf{k}'\mathbf{x}}k'^n\mathrm{d}\mathbf{k}'. \quad (40)$$

The indicated fluctuation average in (40) is performed by expanding the product of the ratios to second order in $\delta T(\mathbf{k}_0)$ and $\delta T(\mathbf{k}'_0)$ as in (3), (7) and (16), and by averaging the products of $\delta T(\mathbf{k}_0)$ and $\delta T(\mathbf{k}'_0)$ as indicated in Section 3.1. In this way, we find

$$\langle G_n(r)\rangle = G_n^{\mathrm{iso}}(r) + \delta G_n^{(1)}(r) + \delta G_n^{(2)}(r) + \mathrm{O}(\delta T^4), \quad (41)$$

where the isotropic leading order $G_n^{\mathrm{iso}}(r)$ is

$$G_n^{\mathrm{iso}}(r) = \frac{s}{(2\pi)^6}\int \frac{1}{\mathrm{e}^{k/T}-1}\frac{1}{\mathrm{e}^{k'/T}-1} \times \mathrm{e}^{\mathrm{i}\mathbf{k}\mathbf{x}}k^n\mathrm{d}\mathbf{k}\mathrm{e}^{-\mathrm{i}\mathbf{k}'\mathbf{x}}k'^n\mathrm{d}\mathbf{k}'. \quad (42)$$

The correction induced by temperature fluctuations can be split into two components:

$$\delta G_n^{(1)}(r) = \frac{s}{(2\pi)^6}\int \frac{1}{\mathrm{e}^{k'/T}-1}\left(\frac{1}{\mathrm{e}^{k/T}-1}\right)_{,T,T} \times\langle\delta T^2(\mathbf{k}_0)\rangle \mathrm{e}^{\mathrm{i}\mathbf{k}\mathbf{x}}k^n\mathrm{d}\mathbf{k}\mathrm{e}^{-\mathrm{i}\mathbf{k}'\mathbf{x}}k'^n\mathrm{d}\mathbf{k}', \quad (43)$$

where $\langle\delta T^2(\mathbf{k}_0)\rangle = \delta_T^2$ in (22) is constant, and

$$\delta G_n^{(2)}(r) = \frac{s}{(2\pi)^6}\int \left(\frac{1}{\mathrm{e}^{k/T}-1}\right)_{,T}\left(\frac{1}{\mathrm{e}^{k'/T}-1}\right)_{,T} \times\langle\delta T(\mathbf{k}_0)\delta T(\mathbf{k}'_0)\rangle \mathrm{e}^{\mathrm{i}\mathbf{k}\mathbf{x}}k^n\mathbf{d}\mathbf{k}\mathrm{e}^{-\mathrm{i}\mathbf{k}'\mathbf{x}}k'^n\mathbf{d}\mathbf{k}', \quad (44)$$

where the temperature correlation $\langle\delta T(\mathbf{k}_0)\delta T(\mathbf{k}'_0)\rangle$ depends on the angular variable $\mathbf{k}_0\mathbf{k}'_0 = \cos\theta$, cf. (20). The subscripts/exponents $n = 0$ and $n = 1$ refer to the number density and energy density correlations, respectively.

4.2 Spatially integrated correlation functions

We integrate the fluctuation-averaged correlation $\langle\rho_n(\mathbf{x})\rangle$ in (39),

$$\int\langle\rho_n(\mathbf{x})\rangle\mathrm{d}\mathbf{x} = \int k^{2n}\langle\mathrm{d}\rho(k,\mathbf{k}_0)\rangle + \int\langle G_n(r)\rangle\mathrm{d}\mathbf{x}, \quad (45)$$

where $\langle\mathrm{d}\rho(k,\mathbf{k}_0)\rangle$ is the averaged spectral density (3) and

$$\int\langle G_n(r)\rangle\mathrm{d}\mathbf{x} = \frac{s}{(2\pi)^3}\int\left\langle\frac{k^{2n}}{(\mathrm{e}^{H(k,\mathbf{k}_0,T)}-1)^2}\right\rangle\mathrm{d}\mathbf{k}, \quad (46)$$

according to (40). The average of the ratio in the integrand is carried out as in (16). The first integral on the right-hand side in (45) is the spatially integrated zero-point divergence in (39). In this way, we find the integrated particle density correlation as

$$\int\langle\rho_{n=0}(\mathbf{x})\rangle\mathrm{d}\mathbf{x} = n(T) + \int\langle G_{n=0}(r)\rangle\mathrm{d}\mathbf{x} = \langle\langle\Delta N^2\rangle_{\mathrm{q}}\rangle/V, \quad (47)$$

and the integrated energy density correlation

$$\int\langle\rho_{n=1}(\mathbf{x})\rangle\mathrm{d}\mathbf{x} = u_2(T) + \int\langle G_{n=1}(r)\rangle\mathrm{d}\mathbf{x} = \langle\langle\Delta U^2\rangle_{\mathrm{q}}\rangle/V. \quad (48)$$

The angular-averaged particle number and internal energy variances $\langle\langle\Delta N^2\rangle_{\mathrm{q}}\rangle$ and $\langle\langle\Delta U^2\rangle_{\mathrm{q}}\rangle$ have been calculated in (17), the specific particle density $n(T)$ is stated in (5), and $u_2(T)$ denotes the average, cf. (4),

$$u_2(T) = \int k^2\langle\mathrm{d}\rho(k,\mathbf{k}_0)\rangle = \frac{4\pi s}{(2\pi)^3}24\zeta(5)T^5\left(1 + 10\frac{\delta_T^2}{T^2}\right). \quad (49)$$

In brief, the spatially integrated correlations reproduce the variances of number count and internal energy.

4.3 Spectral kernels of real-space density correlations

By performing the angular integrations of the isotropic correlation function $G_n^{\rm iso}(r)$ in (42), we find

$$G_n^{\rm iso}(r) = \int_0^\infty g_n^{\rm iso}(r;\omega,\omega')\mathrm{d}\omega\mathrm{d}\omega', \tag{50}$$

$$g_n^{\rm iso}(r;\omega,\omega') = \frac{s}{(\hbar c)^4}\frac{(4\pi)^2}{(2\pi)^6}\frac{\omega^{n+1}}{\mathrm{e}^{\omega/T}-1}\frac{\omega'^{n+1}}{\mathrm{e}^{\omega'/T}-1}\frac{1}{r^2} \times \sin(\omega r)\sin(\omega' r), \tag{51}$$

where we changed the momentum variables k, k' into frequency variables ω, ω' and restored the units. We will use ω[eV], r[cm], $s = 2$, and the CMB mean temperature $T = 2.725\,\mathrm{K}$, so that $g_n^{\rm iso}(r;\omega,\omega')[\mathrm{eV}^{2n-2}/\mathrm{cm}^6]$. In the spectral kernel (51), we substitute $\omega/T \to \omega/(k_{\rm B}T) = \omega[\mathrm{eV}]/(8.617\times10^{-5}T[\mathrm{K}])$ and $\omega r \to \omega r/(\hbar c) = \omega[\mathrm{eV}]r[\mathrm{cm}]/(197.3\times10^{-7})$. The frequency conversion to eV units is $\omega[\mathrm{eV}] = 4.136\times10^{-6}\nu[\mathrm{GHz}]$.

The spectral representation of the correlations $\delta G_n^{(1)}(r)$ and $\delta G_n^{(2)}(r)$ in (41) induced by temperature fluctuations is

$$\delta G_n^{(1)}(r) = \int_0^\infty \delta g_n^{(1)}(r;\omega,\omega')\mathrm{d}\omega\mathrm{d}\omega',$$
$$\delta G_n^{(2)}(r) = \int_0^\infty \delta g_n^{(2)}(r;\omega,\omega')\mathrm{d}\omega\mathrm{d}\omega'. \tag{52}$$

The spectral kernel of $\delta G_n^{(1)}(r)$ reads, after performing the angular integrations in (43),

$$\delta g_n^{(1)}(r;\omega,\omega') = \frac{s}{(\hbar c)^4}\frac{(4\pi)^2}{(2\pi)^6}\frac{\delta_T^2}{2}\left[\frac{\omega'^{n+1}}{\mathrm{e}^{\omega'/T}-1}\left(\frac{\omega^{n+1}}{\mathrm{e}^{\omega/T}-1}\right)_{,T,T} + (\omega\leftrightarrow\omega')\right]\frac{1}{r^2}\sin(\omega r)\sin(\omega' r), \tag{53}$$

where we symmetrized. The units are restored by the substitutions stated after (51), so that $g_n^{(1)}(r;\omega,\omega')[\mathrm{eV}^{2n-2}/\mathrm{cm}^6]$, and δ_T^2/T^2 is dimensionless, see after (25).

The angular integrations of $\delta G_n^{(2)}(r)$ in (44), performed via (29) and (30), give the spectral kernel

$$\delta g_n^{(2)}(r;\omega,\omega') = \frac{s}{(\hbar c)^6}\frac{(4\pi)^2}{(2\pi)^6}\left(\frac{\omega^{n+2}}{\mathrm{e}^{\omega/T}-1}\right)_{,T}\left(\frac{\omega'^{n+2}}{\mathrm{e}^{\omega'/T}-1}\right)_{,T} \times\frac{1}{2\pi}\sum_{l=0}^\infty (l+1/2)C_l j_l(\omega r)j_l(\omega' r). \tag{54}$$

The units are restored as above, and the frequency integrations factorize, cf. Section 5.

The kernel functions $g_n^{\rm iso}$, $\delta g_n^{(1)}$ and $\delta g_n^{(2)}$ are oscillating and slowly decaying $\sim O(1/r^2)$. $g_n^{\rm iso}$ and $\delta g_n^{(1)}$ are finite at $r = 0$, whereas $\delta g_n^{(2)}(r;\omega,\omega') \propto C_1 r^2$, since $j_l(\omega r) \propto r^l$ and $C_0 = 0$, see after (24). In the opposite limit, $j_{2l}(x) \sim (-1)^l\sin(x)/x$ and $j_{2l+1}(x) \sim (-1)^{l+1}\cos(x)/x$. If $\omega = \omega'$ and $\omega r >> 1$, we can average the rapidly oscillating squared angle functions and replace $j_l^2(\omega r)$ by $1/(2\omega^2 r^2)$, so that $\delta g_n^{(2)}(r;\omega,\omega)$ becomes a power law $\propto 1/r^2$ in this limit, and the same holds true for the kernels $\delta g_n^{\rm iso}$ and $\delta g_n^{(1)}$ in (51) and (53) by averaging the squared sine.

5 Frequency-integrated correlations

The isotropic correlation $G_n^{\rm iso}(r)$ in (50) can be evaluated in closed form,

$$G_n^{\rm iso}(r) = s\frac{(4\pi)^2}{(2\pi)^6}I_{0,n}^2(r), \tag{55}$$

as it is defined by the squared integral

$$I_{0,n}(r) = \frac{1}{r}\int_0^\infty \frac{\sin(\omega r)}{\mathrm{e}^{\omega/T}-1}\omega^{n+1}\mathrm{d}\omega = \frac{1}{2\mathrm{i}}\frac{(k_{\rm B}T)^{n+3}}{(\hbar c)^3}\frac{\Gamma(n+2)}{rT} \times\zeta(n+2,1-\mathrm{i}rT) + \mathrm{c.c.}, \tag{56}$$

where ζ denotes the Hurwitz zeta function [27]. The polarization multiplicity in (55) is $s = 2$. Restoring units, we substitute $rT \to rk_{\rm B}T/(\hbar c) = 8.617\times10^{-5}r[\mathrm{cm}]T[\mathrm{K}]/(197.3\times10^{-7})$ and $k_{\rm B}T[\mathrm{eV}] = 8.617\times10^{-5}T[\mathrm{K}]$, also see after (51). As for the CMB radiation, $k_{\rm B}T[\mathrm{eV}] = 2.349\times10^{-4}$ and $rT = 11.90\,r[\mathrm{cm}]$ at $T = 2.725$ K. Thus, $G_n^{\rm iso}(r)[\mathrm{eV}^{2n}/\mathrm{cm}^6]$, where $n = 0$ and $n = 1$ label the number density and energy density correlations, respectively, cf. (37) and (38). The $r = 0$ limit of integral $I_{0,n}(r)$ in (56) is

$$I_{0,n}(r=0) = \frac{(k_{\rm B}T)^{n+3}}{(\hbar c)^3}\Gamma(n+3)\zeta(n+3), \tag{57}$$

so that $G_n^{\rm iso}(r=0)$ is finite.

Temperature fluctuations induce the correction $\delta G_n^{(1)}(r) + \delta G_n^{(2)}(r)$, cf. (41), to be added to the isotropic correlation $G_n^{\rm iso}(r)$, see (52)–(54). The correlation $\delta G_n^{(1)}(r)$ with spectral kernel (53) also admits integration in closed form,

$$\delta G_n^{(1)}(r) = s\frac{(4\pi)^2}{(2\pi)^6}\delta_T^2 I_{0,n}(r)I_{0,n,T,T}(r), \tag{58}$$

where δ_T^2 is defined by the multipole series (22) and δ_T^2/T^2 is a dimensionless constant, cf. after (25). The factor $I_{0,n}(r)$ in (58) is just integral (56), which admits the

temperature derivatives

$$TI_{0,n,T}(r) = \frac{(k_{\rm B}T)^{n+3}}{(\hbar c)^3}\frac{\Gamma(n+3)}{rT}\frac{1}{2{\rm i}}[\zeta(n+2,1-{\rm i}rT) + {\rm i}rT\zeta(n+3,1-{\rm i}rT)] + {\rm c.c.}, \quad (59)$$

and

$$T^2 I_{0,n,T,T}(r) = \frac{(k_{\rm B}T)^{n+3}}{(\hbar c)^3}\frac{\Gamma(n+3)}{rT}\frac{1}{2{\rm i}} \times[(n+1)\zeta(n+2,1-{\rm i}rT) + 2{\rm i}(n+2)rT \times\zeta(n+3,1-{\rm i}rT) - (n+3)(rT)^2 \times\zeta(n+4,1-{\rm i}rT)] + {\rm c.c.} \quad (60)$$

At $r = 0$, these derivatives are finite:

$$TI_{0,n,T}(r=0) = \frac{(k_{\rm B}T)^{n+3}}{(\hbar c)^3}\Gamma(n+4)\zeta(n+3), \quad T^2 I_{0,n,T,T} = (n+2)TI_{0,n,T}. \quad (61)$$

The correlation $\delta G_n^{(2)}(r)$ with kernel (54) reads

$$\delta G_n^{(2)}(r) = s\frac{(4\pi)^2}{(2\pi)^6}\frac{1}{2\pi}\sum_{l=0}^{\infty}(l+1/2)C_l I_{l,n,T}^2(r), \quad (62)$$

where

$$I_{l,n}(r) = \int_0^\infty \frac{\omega^{n+2}}{{\rm e}^{\omega/T}-1} j_l(\omega r){\rm d}\omega, \quad I_{l,n,T}(r) = \int_0^\infty \left(\frac{\omega^{n+2}}{{\rm e}^{\omega/T}-1}\right)_{,T} j_l(\omega r){\rm d}\omega. \quad (63)$$

Integral $I_{l=0,n}(r)$ coincides with $I_{0,n}(r)$ in (56), since $j_0(x) = \sin x/x$. We also note that $\delta G_n^{(2)}(r\to 0) \propto C_1 r^2$, since $C_0 = 0$ and the spherical Bessel functions in (63) vanish $\propto r^l$ at $r = 0$. The units are restored as indicated after (51) and (56); C_l/T^2 is dimensionless and $TI_{l,n,T}[{\rm eV}^n/{\rm cm}^3]$. Figures 3 and 4 show plots of the CMB number density and energy density correlations, their isotropic equilibrium components and their fluctuation corrections. The correlations $G_n^{\rm iso}(r)$ and $\delta G_n^{(1)}(r)$ stay nearly constant up to a distance of $\sim 10^{-2}$ cm (see (64)), and admit power-law asymptotics at large distance, cf. Section 6. The correlation $\delta G_n^{(2)}(r)$, defined by the Bessel series in (62), has an extended crossover regime stretching over four decades in distance. In the case of the energy density correlation depicted in Figure 4, $\delta G_{n=1}^{(2)}(r)$ overpowers the isotropic component $G_{n=1}^{\rm iso}(r)$ at large distance, see Section 6.2.

The correlation function $\langle G_n(r)\rangle$ in (41), composed of the isotropic equilibrium component and the fluctuation corrections, $G_n^{\rm iso} + \delta G_n^{(1)} + \delta G_n^{(2)}$, is finite at $r = 0$,

$$\langle G_n(r=0)\rangle = G_n^{\rm iso}(r=0)\left(1 + \frac{\delta_T^2}{T^2}(n+2)(n+3)\right), \quad (64)$$

and the leading order reads, cf. (55) and (57),

$$G_n^{\rm iso}(r=0) = s\frac{(4\pi)^2}{(2\pi)^6}\frac{(k_{\rm B}T)^{2n+6}}{(\hbar c)^6}\Gamma^2(n+3)\zeta^2(n+3). \quad (65)$$

The δ_T^2/T^2 term in (64) stems from the $\delta G_n^{(1)}(r)$ correction in (58) (with (57) and (61) substituted), and $\delta G_n^{(2)}(r)$ vanishes at $r = 0$, see after (63). The CMB radiation admits $\delta_T^2/T^2 = 1.770\times 10^{-9}$, cf. after (25). As pointed out after (18), the fluctuation average of the squared number count $\langle\langle N\rangle_q^2\rangle$ coincides with the number density correlation $sV^2\langle G_{n=0}(r=0)\rangle$ and factorizes into $\langle\langle N\rangle_q\rangle^2$. The same holds true for the fluctuation-averaged squared internal energy and the energy density correlation, $\langle\langle U\rangle_q^2\rangle = sV^2\langle G_{n=1}(r=0)\rangle = \langle\langle U\rangle_q\rangle^2$.

6 Large-distance asymptotics of the number density and energy density correlations

6.1 Isotropic power-law correlations at large distance

We use the asymptotic expansion of the Hurwitz zeta function $\zeta(n+2,1-{\rm i}rT)$, cf. reference [27], to find the $rT\to\infty$ asymptotics of the isotropic equilibrium correlation $G_n^{\rm iso}(r)$ in (55) defined by integral $I_{0,n}(r)$ in (56),

$$I_{0,n}(r) = \Gamma(n+2)\left[\frac{T{\rm Re}i^n}{(n+1)r^{n+2}} - \frac{{\rm Re}i^{n+1}}{2r^{n+3}} + \frac{B_2}{2!}\frac{\Gamma(n+3)}{\Gamma(n+2)}\frac{{\rm Re}i^{n+2}}{Tr^{n+4}} + \frac{B_4}{4!}\frac{\Gamma(n+5)}{\Gamma(n+2)}\frac{{\rm Re}i^{n+4}}{T^3 r^{n+6}} + \cdots\right]. \quad (66)$$

The B_k are Bernoulli numbers. By specializing this expansion to $n = 0$, we find

$$I_{0,n=0}(r) = \frac{T}{r^2} - \frac{1}{6Tr^4} - \frac{1}{30}\frac{1}{T^3 r^6} + \cdots, \quad (67)$$

so that the long-distance limit of the isotropic number density correlation (55) reads

$$G_{n=0}^{\rm iso}(r) \sim s\frac{(4\pi)^2}{(2\pi)^6}\frac{(k_{\rm B}T)^6}{(\hbar c)^6}\frac{1}{(rT)^4}. \quad (68)$$

The asymptotics of the energy density correlation $G_{n=1}^{\rm iso}(r)$ substantially differs from the number density counterpart $G_{n=0}^{\rm iso}(r)$. At $n = 1$, only the second term in series (66) is non-vanishing, so that $I_{0,n=1}(r) \sim 1/r^4$, up to exponentially small terms ${\rm O}({\rm e}^{-2\pi rT})$. In fact, integral $I_{0,n=1}(r)$ in (56) is elementary,

$$I_{0,n=1}(r) = \frac{1}{r^4} - \pi^3\frac{T^3}{r}\frac{\coth(\pi rT)}{\sinh^2(\pi rT)}. \quad (69)$$

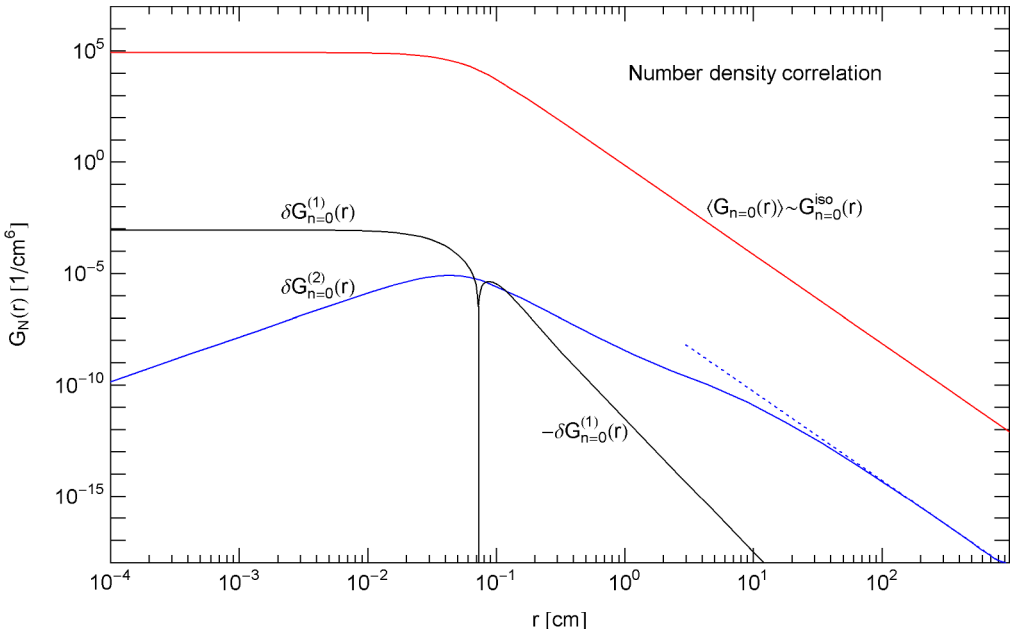

Fig. 3. Number density correlation of the CMB radiation. The red solid curve depicts the isotropic equilibrium correlation $G^{\rm iso}_n(r)$, cf. (55). (The index $n = 0$ labels the number density correlation and $n = 1$ the energy density correlation shown in Fig. 4.) The correlation induced by temperature fluctuations consists of two components $\delta G^{(1)}_n(r) + \delta G^{(2)}_n(r)$, cf. (41). The component $\delta G^{(1)}_{n=0}(r)$ (black solid curve, cf. (58)) becomes negative above the depicted cusp (which extends straight down to zero in this double-logarithmic representation) and decays as $\propto 1/r^6$ at large distance, cf. (71). The second component of the fluctuation correction is the solid blue curve $\delta G^{(2)}_n(r)$, cf. (62). $G^{\rm iso}_{n=0}(r)$ and $\delta G^{(2)}_{n=0}(r)$ admit the same asymptotic power-law decay $\propto 1/r^4$ (indicated by the dotted blue line in the case of $\delta G^{(2)}_{n=0}(r)$), cf. (68) and (76). At short distance, $\delta G^{(2)}_n(r) \propto r^2$. In contrast to the energy density correlation in Figure 4, the isotropic correlation $G^{\rm iso}_{n=0}(r)$ dominates the fluctuation corrections $\delta G^{(1)}_{n=0}(r)$ and $\delta G^{(2)}_{n=0}(r)$ at short as well as large distance, so that the total number density correlation $\langle G_{n=0}(r)\rangle$ in (41) can be approximated by $G^{\rm iso}_{n=0}(r)$.

We thus find the long-distance limit of the energy density correlation (55) as

$$G^{\rm iso}_{n=1}(r) \sim s\frac{(4\pi)^2}{(2\pi)^6}\frac{(k_{\rm B}T)^8}{(\hbar c)^6}\frac{1}{(rT)^8}, \tag{70}$$

to be compared with the much stronger number density correlation (68). Regarding units, see after (56).

6.2 Long-distance correlations generated by angular temperature fluctuations

Temperature fluctuations add the correction $\delta G^{(1)}_n(r) + \delta G^{(2)}_n(r)$ to the isotropic correlation $G^{\rm iso}_n(r)$, cf. Sections 4 and 5. The correlations $\delta G^{(1)}_n(r)$ and $\delta G^{(2)}_n(r)$ have been assembled in (58) and (62). The subscripts $n = 0$ and $n = 1$ label the number density and energy density correlation, respectively.

The large-distance expansion of correlation $\delta G^{(1)}_n(r)$ in (58) is defined by the asymptotic series $I_{0,n}(r)$ in (66). In the case of number density fluctuations, $I_{0,n=0}(r)$ admits the temperature derivatives $TI_{0,n=0,T}(r) \sim T/r^2$ and $T^2 I_{0,n=0,T,T}(r) \sim -1/(3Tr^4)$. We thus obtain, cf. (58),

$$\delta G^{(1)}_{n=0}(r) \sim -s\frac{(4\pi)^2}{(2\pi)^6}\frac{(k_{\rm B}T)^6}{(\hbar c)^6}\frac{\delta_T^2}{T^2}\frac{1}{3(rT)^6}, \tag{71}$$

which anticorrelates in the long-distance limit, see Figure 3. The units are stated after (56).

In contrast, the component $\delta G^{(1)}_{n=1}(r) \sim {\rm O}(e^{-2\pi rT})$ of the energy density correlation is exponentially decaying (and also negative) in the long-distance limit, see Figure 4, since the temperature derivatives $TI_{0,n=1,T}(r)$ and $T^2 I_{0,n=1,T,T}(r)$ are exponentially small, cf. (69).

To obtain the $rT \gg 1$ asymptotics of the correlation $\delta G^{(2)}_n(r)$ in (62) determined by the Bessel integrals $I_{l,n}(r)$ in (63), we expand the ratio in the integrand of $I_{l,n}(r)$ into an ascending Bernoulli series and use term-by-term integration with an exponential convergence factor (which can subsequently be dropped) to obtain

$$I_{l,n}(r) = \frac{\pi}{2^{l+1}}\frac{T}{r^{n+2}}\sum_{k=0}^{\infty}\frac{B_k}{k!}\frac{\gamma(l,n,k)}{(rT)^k}, \tag{72}$$

$$\gamma(l,n,k) := \frac{\Gamma(l+n+k+2)}{\Gamma((l-n-k+1)/2)\Gamma((l+n+k+3)/2)}, \tag{73}$$

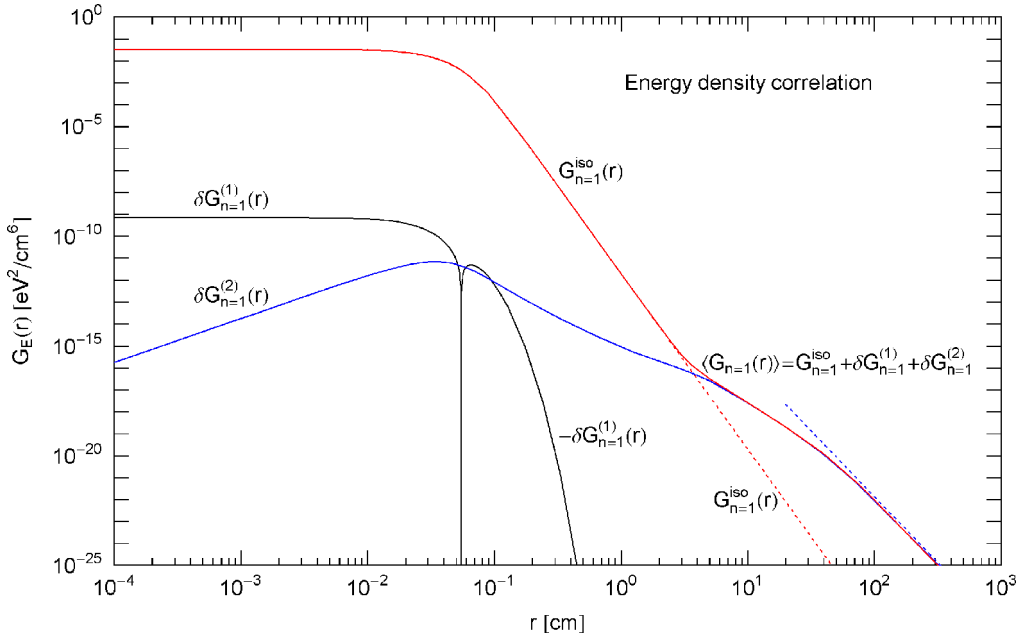

Fig. 4. Energy density correlation of the CMB radiation. The total correlation $\langle G_{n=1}(r)\rangle$ is depicted as red solid curve and consists of three components $G^{\rm iso}_{n=1}(r) + \delta G^{(1)}_{n=1}(r) + \delta G^{(2)}_{n=1}(r)$, cf. (41). (The subscript $n = 1$ labels the energy density correlation.) The isotropic component $G^{\rm iso}_{n=1}(r)$ is the upper extension of the red dotted line and decays $\propto 1/r^8$ at large distance, cf. (55) and (70). Temperature fluctuations generate the corrections $\delta G^{(1)}_{n=1}(r)$ (black solid curve) and $\delta G^{(2)}_{n=1}(r)$ (blue solid curve), cf. (58) and (62). The correction $\delta G^{(1)}_{n=1}(r)$ becomes negative above the depicted cusp and decays exponentially at large r, cf. after (71). The second fluctuation correction $\delta G^{(2)}_{n=1}(r)$ decays $\propto 1/r^6$ (blue dotted line), cf. (77), and overpowers the isotropic correlation $G^{\rm iso}_{n=1}(r) \propto 1/r^8$ (red dotted line) at large distance.

where l and n are non-negative integers. The temperature derivative thereof reads

$$TI_{l,n,T} = \frac{\pi}{2^{l+1}} \frac{(k_{\rm B}T)^{n+3}}{(\hbar c)^3} \sum_{k=0}^{\infty} \frac{B_k}{k!}(1-k)\frac{\gamma(l,n,k)}{(rT)^{k+n+2}}. \quad (74)$$

The units of $TI_{l,n,T}[{\rm eV}^n/{\rm cm}^3]$ can be restored as indicated after (56). The leading order of $I_{l,n,T}$ is the $k = 0$ term if $l > n-1$ or $l = n-1-(2m+1)$, $m = 0, 1\ldots$. If both of these conditions are not met (e.g., $l = 0$, $n = 1$), all terms in series (74) vanish and the decay is exponential. Accordingly,

$$\begin{aligned} TI_{l,n=0,T}(r) &\sim \frac{\pi}{2^{l+1}} \frac{(k_{\rm B}T)^3}{(\hbar c)^3} \frac{\gamma(l,0,0)}{(rT)^2}, \\ TI_{l,n=1,T}(r) &\sim \frac{\pi}{2^{l+1}} \frac{(k_{\rm B}T)^4}{(\hbar c)^3} \frac{\gamma(l,1,0)}{(rT)^3}, \end{aligned} \quad (75)$$

except for the decay of $TI_{l=0,n=1,T}(r)$ which is exponential of ${\rm O}({\rm e}^{-2\pi rT})$, cf. (69). (Since $C_0 = 0$ in (62), this term drops out.) The long-distance power-law asymptotics of correlation $\delta G^{(2)}_n(r)$ in (62) is obtained by substituting these limits:

$$\begin{aligned} \delta G^{(2)}_{n=0}(r) \sim\ & s\frac{(4\pi)^2}{(2\pi)^6}\frac{(k_{\rm B}T)^6}{(\hbar c)^6}\frac{1}{(rT)^4} \\ & \times \sum_{l=1}^{\infty}(l+1/2)\frac{C_l}{T^2}\frac{\pi}{2^{2l+3}}\gamma^2(l,0,0), \end{aligned} \quad (76)$$

$$\begin{aligned} \delta G^{(2)}_{n=1}(r) \sim\ & s\frac{(4\pi)^2}{(2\pi)^6}\frac{(k_{\rm B}T)^8}{(\hbar c)^6}\frac{1}{(rT)^6} \\ & \times \sum_{l=1}^{\infty}(l+1/2)\frac{C_l}{T^2}\frac{\pi}{2^{2l+3}}\gamma^2(l,1,0), \end{aligned} \quad (77)$$

with $\gamma(l,n,k)$ in (73). In the double-logarithmic plots in Figures 3 and 4, these power laws are indicated as dotted straight lines. As for the energy density correlation (see Figure 4), the fluctuation correction $\delta G^{(2)}_{n=1}(r) \propto 1/r^6$ in (77) overpowers the isotropic equilibrium correlation $G^{\rm iso}_{n=1}(r) \propto 1/r^8$ (cf. (70)) in the long-distance limit, whereas $\delta G^{(1)}_{n=1}(r)$ decays exponentially, cf. after (71). This is in contrast to the number density correlation depicted in Figure 3, where $G^{\rm iso}_{n=0}(r)$ in (68) and $\delta G^{(2)}_{n=0}(r)$ in (76) decay with the same power $1/r^4$, and $\delta G^{(1)}_{n=0}(r) \propto 1/r^6$, cf. (71).

7 Conclusion

We studied the effect of angular temperature fluctuations on the thermodynamic variables and real-space correlation functions of a photon gas. We considered a specific example, the cosmic microwave background (CMB) radiation, where detailed measurements of the temperature multipole spectrum are available, which determine the partition function of this stationary non-equilibrium system and allowed us to quantify the fluctuation corrections of the internal energy, entropy, heat capacity and compressibility, cf. Section 2. The magnitude of the fluctuation correction is determined by a dimensionless parameter δ_T^2/T^2, where T is the mean temperature and the constant δ_T^2 is defined by the weighted series $\sum_{l=1}^{\infty}(l+1/2)C_l/(2\pi)$ of the measured multipole coefficients, cf. (22). In the case of the CMB radiation, the fluctuation corrections are sufficiently small to treat them perturbatively by expanding the thermodynamic variables in powers of $\delta_T^2/T^2 \sim 1.770 \times 10^{-9}$ around the equilibrium state.

Figures 1 and 2 depict the multipole coefficients C_l of the temperature pair correlation $\langle \delta T(\mathbf{k}_0)\delta T(\mathbf{k}_0')\rangle$ up to multipoles of order $l \sim 2500$, where the above series is truncated. The low-l coefficients depicted in Figure 2 have large error bars due to cosmic variance, taking account of the fact that there is only one configuration of the random field $\delta T(\mathbf{k}_0)$ measured which is used in the angular average (19) and in the calculation of the multipole coefficients (23), cf. references [3,28]. Since the low-l multipoles significantly enter in the above series defining δ_T^2/T^2, we performed a least-squares χ^2 fit of the power spectrum depicted in Figure 1, which admits a narrow 1σ error band at low multipoles, cf. Figure 2. To calculate the constant δ_T^2/T^2, we used the analytic representation (25) of the C_l employed in the spectral fit, a series of eight Gaussians rescaled with a power-law scale factor, cf. Table 1. This analytic representation covers the complete multipole spectrum measured by the Planck satellite [3]. In the Planck data set, the entire dipole moment has been subtracted, as it is regarded as Doppler shift generated by the motion of the Earth in the rest frame of the background radiation [29,30]. However, there is a small intrinsic dipole which can be obtained by extrapolating the χ^2 fit of the C_l to $l = 1$, cf. Section 3.1.

In Sections 3–6, we studied the real-space counterpart to the temperature correlation function $\langle \delta T(\mathbf{k}_0)\delta T(\mathbf{k}_0')\rangle$ on the sphere $\mathbf{k}_0^2 = 1$ in momentum space. In Section 3, we explained the angular Fourier transform which maps the multipole expansion of $\langle \delta T(\mathbf{k}_0)\delta T(\mathbf{k}_0')\rangle$ on the unit sphere into a Bessel series in real space, cf. (20) and (54). The latter defines the frequency- and distance-dependent spectral kernels of the number density and energy density correlations induced by temperature fluctuations, cf. Section 4.3.

In Sections 5 and 6, we discussed the frequency-integrated density correlations of the CMB radiation. Both the number density and energy density correlations stay nearly constant at short distance, up to $r \leq 10^{-2}$ cm, see the double-logarithmic plots of the correlation functions in Figures 3 and 4. (The number density of the CMB radiation is just 411 photons/cm^3 [31].) The fluctuation-induced corrections to the number and energy density correlations of the equilibrium state show an extended crossover (defined by the frequency-integrated Bessel series (54)), stretching over four orders in distance and terminating in power-law decay. The isotropic equilibrium correlation of the number density and its fluctuation correction decay with the same power law $\propto 1/r^4$, whereas the equilibrium component of the energy density correlation decays as $1/r^8$ and is dominated by the fluctuation-induced component $\propto 1/r^6$, see Figures 3 and 4.

References

1. Planck Collaboration, Astron. Astrophys. **594**, A1 (2016)
2. Planck Collaboration, Astron. Astrophys. **594**, A11 (2016)
3. Planck Legacy Archive, Release PR2, 2015, Available at: http://pla.esac.esa.int/pla/
4. G.-H. Liu, W. Li, G. Su, G.-S. Tian, Eur. Phys. J. B **87**, 105 (2014)
5. G.-H. Liu, L.-J. Kong, W.-L. You, Eur. Phys. J. B **88**, 284 (2015)
6. M. Wang, S.-J. Ran, T. Liu, Y. Zhao, Q.-R. Zheng, G. Su, Eur. Phys. J. B **89**, 27 (2016)
7. L. Pan, D. Zhang, H.-H. Hung, Y.-J. Liu, Eur. Phys. J. B **90**, 105 (2017)
8. S. Tarat, P. Majumdar, Eur. Phys. J. B **88**, 68 (2015)
9. W.C. Yu, S.-J. Gu, H.-Q. Lin, Eur. Phys. J. B **89**, 212 (2016)
10. Y. Fujiki, S. Mizutaka, K. Yakubo, Eur. Phys. J. B **90**, 126 (2017)
11. Y. Zhang, X. Li, Eur. Phys. J. B **88**, 61 (2015)
12. A. Mehri, S.M. Lashkari, Eur. Phys. J. B **89**, 241 (2016)
13. Y. Matsubara, Y. Hieida, S. Tadaki, Eur. Phys. J. B **86**, 371 (2013)
14. P. Wang, Z. Chang, H. Wang, H. Lu, Eur. Phys. J. B **90**, 214 (2017)
15. R. Tomaschitz, Physica A **483**, 438 (2017)
16. R. Tomaschitz, Astropart. Phys. **84**, 36 (2016)
17. Pierre Auger Collaboration, J. Cosmol. Astropart. Phys. **JCAP06**, 026 (2017)
18. IceCube Collaboration, Astrophys. J. **826**, 220 (2016)
19. HAWC Collaboration, Astrophys. J. **796**, 108 (2014)
20. L.D. Landau, E.M. Lifshitz, *Quantum mechanics: non-relativistic theory*, 3rd edn. (Pergamon, London, 1991)
21. R.G. Newton, *Scattering theory of waves and particles* (Springer, New York, 1982)
22. G.N. Watson, *A treatise on the theory of Bessel functions* (Cambridge University Press, Cambridge, 1996)
23. A.D. Jackson, L.C. Maximon, SIAM J. Math. Anal. **3**, 446 (1972)
24. R. Mehrem, Appl. Math. Comput. **217**, 5360 (2011)
25. V.I. Fabrikant, Quart. Appl. Math. **71**, 573 (2013)
26. L.D. Landau, E.M. Lifshitz, *Statistical physics*, 3rd edn. (Pergamon, Oxford, 1980)
27. F.W.J. Olver, D.W. Lozier, R.F. Boisvert, C.W. Clark (Eds.), *NIST Digital Library of Mathematical Functions*, Release 1.0.16, 2017, Availbale at: http://dlmf.nist.gov
28. R. Tomaschitz, Mon. Not. R. Astron. Soc. **427**, 1363 (2012)
29. Planck Collaboration, Astron. Astrophys. **571**, A27 (2014)
30. Pierre Auger Collaboration, Science **357**, 1266 (2017)
31. C. Patrignani et al., Chin. Phys. C **40**, 100001 (2016)